Electron-paramagnetic-resonance identification of a trigonal manganese-indium pair in silicon

J. Kreissl and W. Gehlhoff
Academy of Sciences of the German Democratic Republic, Center for Scientific Instruments, Rudower Chaussee 6, Berlin 1199, German Democratic Republic

P. Omling and P. Emanuelsson
Department of Solid State Physics, University of Lund, Box 118, S-221 00 Lund, Sweden
(Received 29 March 1990)

A new, defect-related electron-paramagnetic-resonance (EPR) spectrum in silicon doped with indium and manganese is reported. The spectrum shows trigonal symmetry, and the involvements of Mn and In in the defect are proven from the observed hyperfine interactions. A complicated and unusual fine-structure behavior shows that the zero-field splitting and Zeeman energies are of similar magnitude, a so-called intermediate case. The analysis of the experimental data gives strong evidence that the microscopic nature of the defect identifies it as being a nearest-neighbor pair of interstitial Mn and substitutional In, and that the EPR spectrum originates from the $^6S_{5/2}$ ground state of the Mn^{2+} ion in a crystal field of cubic symmetry with a strong trigonal distortion, i.e., from a $(Mn_i^{2+}\ In_s^{-})$ pair.

I. INTRODUCTION

Manganese is one of the most extensively studied transition-metal (TM) impurities in silicon and has played an important role for the understanding of such defects. The information on Mn has been obtained from many different experiments. Electron-paramagnetic-resonance (EPR) investigations have given detailed information on the identity, symmetry, and electronic structure,[1] while combined EPR and neutron activation measurements have determined the temperature-dependent solubility.[2] From space-charge measurements the electronic properties of the defects have been characterized,[3,4] and the electronic structure has been analyzed from optical data.[5,6] Of special interest is the pioneering EPR investigation by Ludwig and Woodbury,[1] which showed that isolated manganese can exist in different charged states, both in interstitial (Mn_i^{-}, Mn_i^0, Mn_i^{+}, and Mn_i^{2+}) and substitutional (Mn_s^{2-} and Mn_s^{+}) lattice sites. This information, together with data obtained on other TM impurities, was used to suggest a model by which the electronic configuration of the TM impurities could be predicted. These, and later experimental and more fundamental theoretical studies, have resulted in a comprehensive picture of the electronic structure of isolated Mn.[7,8]

From EPR investigations it is also well known that Mn, alone or in combination with other impurities or defects, forms different types of complexes. The type and concentration of these complex defects depend strongly on the heat treatment, cooling procedure, and concentration of background impurities in the silicon crystal. One such Mn complex is the Mn_4^0 cluster, which was recently investigated in detail by EPR.[9] Other examples are the pairs between Mn and different impurities. Of these, the MnAu, MnPt, MnB, MnAl, and MnZn pairs were discovered and identified by Ludwig and Woodbury,[1] while the MnCu pair was studied by Dietrich *et al.*[10]

The successful exploration of pairs of iron and group-III acceptors[11–13] has resulted in a renewed interest in EPR investigations of the corresponding Mn-acceptor pairs. For instance, the question whether or not the Mn-acceptor pairs show metastable properties similar to the Fe-acceptor pairs is of considerable interest. So far, the EPR spectra of $(MnB)^{+}$ and $(MnAl)^{+}$ have been observed,[1,14] but only the $(MnB)^{+}$ pair has been investigated in more detail.[14] The spectra both show trigonal symmetry, and are interpreted as being due to a nearest-neighbor (NN) pair of Mn_i^{2+} and B_s^{-} and Al_s^{-}, respectively. The spectra are successfully analyzed using a spin Hamiltonian with $S=\frac{5}{2}$, corresponding to a model in which the spin properties originate from the $^6S_{5/2}$ ground state of a Mn^{2+} ion in a trigonally distorted cubic crystal field.[14] The next-nearest-neighbor (NNN) configuration, as was reported for the neutral $(Fe_i^{+}A_s^{-})$ pairs (with A=Al,Ga,In),[11,12,15] has not, however, been observed for the positively charged manganese-acceptor centers. The electric behavior of the (MnB) pair has been characterized by space-charge techniques[3] and a combination of space-charge and EPR investigations,[16] and the position of the $(MnB)^{+/0}$ energy level has been determined to be $E_c-0.5$ eV. Similar midgap positions have been reported for the corresponding MnAl and MnGa levels.[17]

In contrast to the other Mn-acceptor pairs, no experimental data on the MnIn pair have ever been reported. We have searched, therefore, for such a defect by codoping Si samples with Mn and In. A new EPR spectrum, showing great complexity, has thus been discovered. In this paper the new spectrum will be identified as a trigonal pair of Mn and In, and the analysis will show that the spectrum arises from the ground-state manifold of the $(Mn^{2+}In^{-})$ defect.

II. EXPERIMENT

The samples were prepared from Czochralski grown, indium-doped, silicon crystals with an In content of about 10^{17} cm^{-3}. The manganese doping was performed by encapsulating a small piece of metallic manganese and a carefully etched {110} oriented Si:In sample in an evacuated quartz ampule. The ampule was heat treated for 1 h at 1150 °C. After the diffusion process the sample was rapidly quenched by dropping the ampule into water.

The EPR measurements were performed at the X band using a ZWG ERS 230 spectrometer equipped with a fixed temperature cryostat ($T=20.4$ K) and a Bruker ESP 300 spectrometer equipped with a He gas-flow cryostat for variable temperature measurements.

III. EXPERIMENTAL RESULTS AND ANALYSIS

In samples codoped with Mn and In a complicated EPR spectrum was observed. The spectrum, which depends strongly on the angle between the crystal axes and the magnetic field, is shown for the three main directions ($\mathbf{B}\|\langle 110\rangle$, $\langle 111\rangle$, and $\langle 100\rangle$) in Fig. 1. The sixfold hyperfine splitting observed in these main directions clearly shows the involvement of one Mn atom ($I=\frac{5}{2}$, 100% natural abundance) in the defect. A closer inspection of the high-field line group in the $\mathbf{B}\|\langle 111\rangle$ direction (see Fig. 2) reveals a further splitting of each Mn hyperfine line into ten components. This proves the hyperfine interaction with one In atom. The indium isotopes ^{113}In (4.28% natural abundance) and ^{115}In (95.72% natural abundance) both have nuclear spin $I=\frac{9}{2}$, and, since their gyromagnetic ratio is close to unity, they will effectively give rise to only one tenfold hyperfine splitting. This reasoning assumes that only the allowed nuclear spin transitions ($\Delta m_{\mathrm{In}}=0$) are of importance, and, as will be shown later, this is actually the case in this particular direction. In Fig. 2, a stick spectrum is also drawn, which shows, firstly, the positions of the hyperfine transitions caused by Mn (dashed lines) and, secondly, the positions caused by the further splitting due to In (small solid lines). For clarity the stick spectra for In have been drawn only for the outer lines. The intensity variation of the experimental lines in Fig. 2 is a result of the overlap between hyperfine split lines of In. For arbitrary directions the manganese and indium hyperfine interactions become very complicated because of the simultaneous occurrence of allowed and forbidden hyperfine transitions. This is due to a strong mixing of the nuclear states. In the case of indium this mixing is due to the fact that the hyperfine, the quadrupole, and the nuclear Zeeman in-

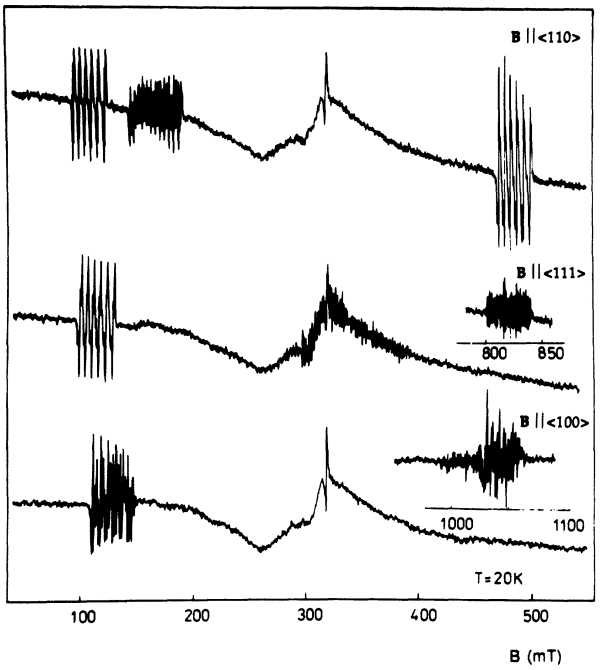

FIG. 1. Experimental EPR spectra of the ($Mn^{2+}In^{-}$) pair for the three main directions, obtained at $T=20$ K and using a microwave frequency of 9.01 GHz. The single resonance at 320 mT is due to the surface signal.

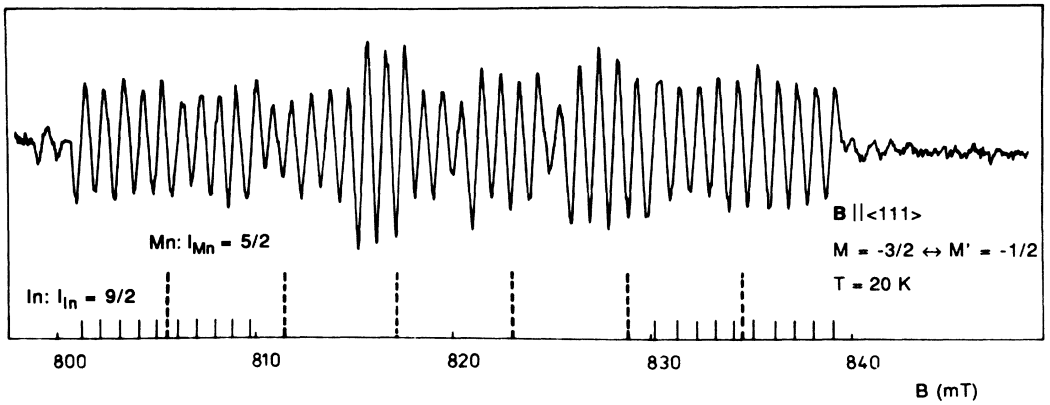

FIG. 2. Hyperfine splitting of the fine-structure transition $M=-\frac{3}{2}\leftrightarrow M'=-\frac{1}{2}$ for $\mathbf{B}\|\langle 111\rangle$ ($\theta=0°$) at $T=20$ K. The dashed lines of the stick spectrum show the sixfold splitting caused by the manganese hyperfine interaction. Each of those lines are further split into 10 lines by the indium hyperfine interactions (indicated as small solid lines). For simplicity that splitting is only shown for the two outer manganese hyperfine transitions.

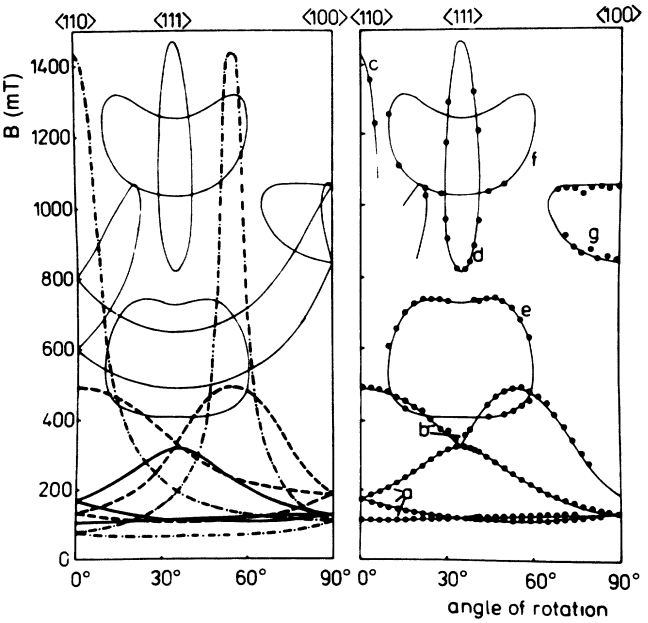

FIG. 3. Angular dependence of fine-structure line positions of the ($Mn_i^{2+}In_s^-$) pair obtained at 9.01 GHz. The magnetic field is rotated in a crystal {110} plane. Left side: A plot of all possible fine-structure transitions. The bold lines reflect transitions within the three Kramers doublets (solid bold lines for transitions within the $|\pm\frac{1}{2}\rangle$ doublet, dashed bold lines for transitions within the $|\pm\frac{3}{2}\rangle$ doublet, and dotted-dashed bold lines for transitions within the $|\pm\frac{5}{2}\rangle$ doublet). The thin solid lines show transitions between different Kramers doublets. Right side: The experimental data are given by solid circles. In order to facilitate a comparison with the left figure, the parts of the calculated angular dependence for which experimental data exist are indicated by thin solid lines. The letters show the different parts of the fine-structure transitions which are described in Sec. III.

teractions have comparable strengths. In the case of manganese the mixing is caused by the effective magnetic field acting on the manganese nucleus, which is dependent on the electronic spin, and which is created by the comparable electronic Zeeman and zero-field interactions. In this latter case the manganese hyperfine pattern depends on the quantum number of the electronic spin transition. This was extensively studied for the ($Mn_i^{2+}B_s^-$) pair.[14] The intensity of all forbidden transitions is equal to zero when the magnetic field is oriented exactly along the z (trigonal) direction of the defect. But already a small misalignment gives measurable intensities of the forbidden ($\Delta m=\pm1$) nuclear spin transitions of manganese. Because of such a small misalignment, weak forbidden lines outside of the allowed hyperfine transitions can be observed in Fig. 2. The line positions of these forbidden transitions can only be understood for an electronic spin transition from $M=\pm\frac{3}{2}$ to $M'=\pm\frac{1}{2}$, since the theory predicts that only in that case do two of the ten forbidden ($\Delta m\pm1$) manganese nuclear spin transitions fall outside the six allowed ones. The complete analysis of the hyperfine interactions will be presented in a later publication. We do conclude, however, that the observed hyperfine interactions prove that the defect contains one Mn and one In atom.

The measured angular dependence of the electronic spin transitions is plotted as solid circles on the right side of Fig. 3. The solid circles represent the fine-structure positions, which have been estimated as the center of gravity of the measured hyperfine structure transitions. The intensity of the transitions depends strongly on the angle. Therefore, in many cases the lines cannot be observed for all directions. The low field resonance pattern (between 0 and 330 mT, denoted a in Fig. 3) indicates a trigonal symmetry and, using the simple spin Hamiltonian $H=\mu_B\mathbf{B}\cdot\vec{g}'\cdot\mathbf{S}'$, the effective g' values (assuming $S'=\frac{1}{2}$) were determined to be $g'_\parallel=2.00$ and $g'_\perp=5.82$. This behavior is expected for transitions within a $|\pm1/2\rangle$ doublet of a trigonally distorted spin-$\frac{5}{2}$ system with a large zero-field splitting (characterized by the zero-field splitting parameter D). In the strong zero-field limit ($D\gg g\mu_B B$), the expected g' values would be $g'_\parallel=2$ and $g'_\perp=6$. However, the deviation from $g'_\perp=6$, and the observation of several groups of lines in Fig. 3 suggests that the fine-structure splitting is not dominating over the Zeeman splitting in the experiment.

From the observations described above, it can be concluded (a more-detailed motivation will be given below) that the spectrum is caused by electronic spin transitions within a $^6S_{5/2}$ ground state of a $3d^5$ manganese ion which experiences a trigonal distortion of the cubic crystal field from an associated indium ion. The spin Hamiltonian of such a manganese-indium pair can be written as (neglecting the quadrupole and nuclear Zeeman hyperfine terms discussed above)[14,18]

$$H=H_{\rm CF}+H_Z+H_{\rm Mn}+H_{\rm In}\ , \tag{1}$$

$$H_{\rm CF}=D[S_z^2-(\tfrac{1}{3})S(S+1)]-[(a-F)/180][35S_z^4-30S(S+1)S_z^2+25S_z^2-6S(S+1)+3S^2(S+1)^2]$$
$$+\frac{\sqrt{2}}{36}a[S_z^2(S_+^3+S_-^3)+(S_+^3+S_-^3)S_z^2]\ , \tag{2}$$

$$H_Z=g_\parallel\mu_B B_z S_z+g_\perp\mu_B(S_xB_x+S_yB_y)\ , \tag{3}$$

$$H_{\rm Mn}=A_{\rm Mn}I_z^{\rm Mn}S_z+B_{\rm Mn}(S_xI_x^{\rm Mn}+S_yI_y^{\rm Mn})\ , \tag{4}$$

$$H_{\rm In}=A_{\rm In}I_z^{\rm In}S_z+B_{\rm In}(S_xI_x^{\rm In}+S_yI_y^{\rm In})\ , \tag{5}$$

where all symbols have their usual meanings. A convenient way to analyze the spectrum in this formalism is to apply perturbation theory. This is possible in our case since the zero-field splitting energy is large compared to the Zeeman and hyperfine splittings for the transitions within the $|\pm\frac{1}{2}\rangle$ Kramers doublet. The information from such a perturbation treatment has, in fact, already been used to determine the symmetry and spin state of the defect. The perturbation theory is, furthermore, useful for an estimation of the zero-field parameter D. Such an estimated value can be used as an initial value for the procedure of exact diagonalization of the energy matrix used later, a procedure which is necessary for a description of the whole angular dependence. Using perturbation theory up to the third order and neglecting the hyperfine interactions, it can be shown that the experimental g' value of a transition within the $|\pm\frac{1}{2}\rangle$ doublet of an orbital singlet system with spin S has the following angular dependence:[19]

$$g'(\theta)=[g_{\parallel}^2+(k^2g_{\perp}^2-g_{\parallel}^2)\sin^2\theta]^{1/2} \times\{1-(n^2/4)[(g_{\perp}\mu_B B)/(2D)]^2F(\theta)\} \quad (6)$$

with

$$k=[S(S+1)+1/4]^{1/2}\,, \quad (7)$$

$$n=[S(S+1)-3/4]^{1/2}\,, \quad (8)$$

and

$$F(\theta)=\sin^2\theta\{[(k^2g_{\perp}^2+2g_{\parallel}^2)\sin^2\theta -2g_{\parallel}^2]/[(k^2g_{\perp}^2-g_{\parallel}^2)\sin^2\theta+g_{\parallel}^2]\}\,. \quad (9)$$

With the magnetic field oriented along the trigonal crystal axis, i.e., $\theta=0$, Eq. (2) reduces to $g'=g_{\parallel}$, while at $\theta=\pi/2$, Eq. (2) gives for $S=\frac{5}{2}$

$$g_{\perp}'=3g_{\perp}\{1-2[g_{\perp}\mu_B B/(2D)]^2\}\,. \quad (10)$$

In order to determine the three parameters $g_{\parallel}$, $g_{\perp}$, and D, it is necessary either to measure the spectrum at two different microwave frequencies or to measure g' at some intermediate angle to a very high accuracy. The first alternative was not possible, and the second alternative is not realistic in our case due to the uncertainty in line position and angle determination. Since our purpose at the moment is only to estimate the zero-field splitting parameter, we use the approximation that the real $g_{\parallel}$ and $g_{\perp}$ values are both close to 2, which is indeed expected for an S ground state. From Eq. (10) it is now straightforward to estimate that $|D|\approx 0.5\ \mathrm{cm}^{-1}$. This simple calculation shows that the energy of the zero-field splitting for the MnIn system is of the same order of magnitude as the Zeeman energy at the resonances and, consequently, an analysis of all transitions using perturbation theory is not suitable for this system.

In order to proceed we have applied the method of direct diagonalization of the $S=\frac{5}{2}$ energy matrix. Using a computer procedure for the calculation of eigenvalues and eigenfunctions for a Hamiltonian, including the crystal field and the electronic Zeeman interactions [Eqs. (2) and (3)], a good agreement between the measured and calculated line positions and intensities could be obtained for the whole angular dependence of the fine-structure transitions. The results of the theoretical calculations are shown in Fig. 3. On the left side all possible EPR transitions are included as solid bold lines for transitions within the $|\pm\frac{1}{2}\rangle$ doublet, dashed bold lines for transitions within the $|\pm\frac{3}{2}\rangle$ doublet, dotted-dashed bold lines for transitions within the $|\pm\frac{5}{2}\rangle$ doublet, and thin solid lines for transitions between different Kramers doublets. On the right side of Fig. 3, the calculated curves for which experimental data exist are included as thin lines in order to show the good agreement between theory and experiment. The parameters $g_{\parallel}$, $g_{\perp}$, D, and $a-F$, which were found to give the best fit of the experimental points, are given in Table I. The hyperfine constants determined in the main directions are also included in Table I.

In the following discussion of the results of the calculations it should be noted that the good quantum numbers in the low-magnetic-field region differ from those in the high-magnetic-field region. Of course, in the range in which most of the spin transitions occur, there are no good quantum numbers, but in order to keep track of the energy levels in the discussion we will designate them with the low field quantum numbers.

The energy structure of the ground-state multiplet of the $^6S_{5/2}$ system as a function of magnetic field has been deduced from the calculation of the energy matrix, and the results for the magnetic field along the high symmetry axes are plotted in Figs. 4 and 5. The line group denoted by a in Figs. 3–5, corresponding to transitions within the $|\pm\frac{1}{2}\rangle$ doublet, has already been discussed above in the frame of perturbation theory. A second group of transitions, denoted b in Figs. 3–5, is identified as a transition within the $|\pm\frac{3}{2}\rangle$ Kramers doublet. In agreement with the experimental results, this transition has, according to the calculations, no measurable transition probability for the magnetic field oriented along the trigonal axis. It is, however, allowed in other directions, particularly in the perpendicular direction where the states are extremely mixed.

In principle the same arguments as for the transitions within the $|\pm\frac{3}{2}\rangle$ doublet are valid for transitions within the $|\pm\frac{5}{2}\rangle$ doublet, labeled c in Fig. 5. The transition probability, however, is smaller for the transitions within the $\pm\frac{5}{2}\rangle$ doublet. Therefore, only a small part of the angular dependence around $\mathbf{B}\|\langle 110\rangle$ is measurable.

At higher magnetic fields ($B>400$ mT) the Zeeman en-

TABLE I. Spin Hamiltonian parameters of the $(Mn_i^{2+}In_s^{-})$ pair.

$g_{\parallel}$	2.005±0.005
$g_{\perp}$	2.005±0.005
D	0.520±0.005 cm^{-1}
a-F	0.015±0.002 cm^{-1}
$\lvert A_{\mathrm{Mn}}\rvert$	$(54.9\pm0.5)\times10^{-4}$ cm^{-1}
$\lvert B_{\mathrm{Mn}}\rvert$	$(53.7\pm0.5)\times10^{-4}$ cm^{-1}
$\lvert A_{\mathrm{In}}\rvert$	$(9.0\pm0.1)\times10^{-4}$ cm^{-1}
$\lvert B_{\mathrm{In}}\rvert$	$\leq 3\times10^{-4}$ cm^{-1}

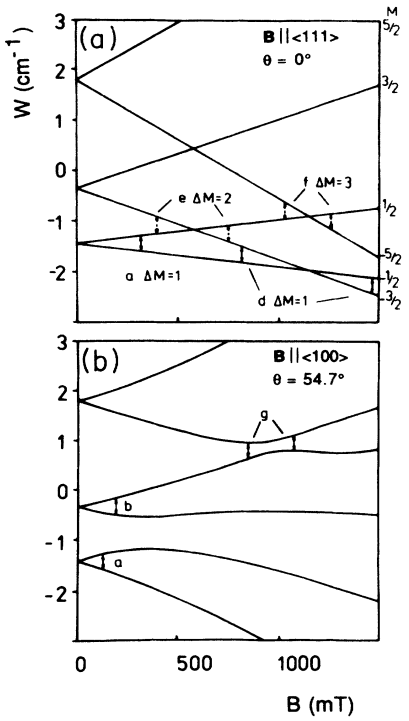

FIG. 4. Energy-level diagrams for the $(Mn_i^{2+}In_s^-)$ pair for (a) the trigonal direction ($\theta=0°$) and (b) for $\theta=54.7°$. EPR transitions at 9.01 GHz are indicated, and designated in accordance with Fig. 3 and Sec. III.

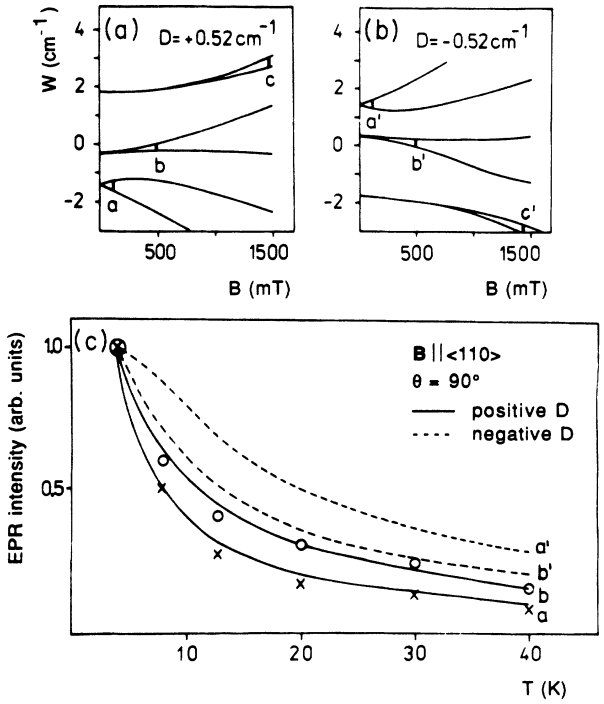

FIG. 5. Determination of the sign of the zero-field splitting parameter D of the $(Mn_i^{2+}In_s^-)$ pair from an investigation of EPR line intensities. The figure presents energy-level diagrams assuming in (a) a positive sign, and in (b) a negative sign of D. (c) shows a comparison between the experimental and the calculated temperature dependence of the line intensities (solid lines for positive D and dashed lines for negative D) for the two fine-structure transitions a (or a') and b (or b'). The experimental data, which are drawn as crosses (for a or a') and open circles (for b or b'), show that D is positive.

ergies at the resonances are of the same magnitude as the fine-structure energy, and in this intermediate range both allowed and forbidden electronic spin transitions can be expected. The allowed transitions are characterized by $\Delta M=\pm1$ and the forbidden ones by $\Delta M=\pm2,\pm3,\pm4,\pm5$ for the $S=\frac{5}{2}$ system. For the magnetic field oriented along the trigonal symmetry axis of a defect there is no mixing of states (neglecting the small contributions, in our case, to the zero-field splitting from the fourth-order spin terms). Therefore, independently of the strength of the Zeeman and crystal-field interactions, M is always a good quantum number. In this particular direction only transitions with $\Delta M=1$ exist (and $\Delta m_I=0$, see Fig. 2 and the corresponding discussion). The $\Delta M=1$ transitions $M=\frac{1}{2}\leftrightarrow M'=-\frac{1}{2}$ and $M=-\frac{1}{2}\leftrightarrow M'=-\frac{3}{2}$ are, in Figs. 3 and 4, denoted a and d, respectively. The identification of the d transition is furthermore verified by the observation of forbidden nuclear $\Delta m=\pm1$ transitions, as was discussed above in connection to the identification of the hyperfine lines in Fig. 2.

If the magnetic field axis is moved away from the trigonal crystal axis, the calculations show that a mixing of states occurs, resulting in measurable transition probabilities for the forbidden transitions with $\Delta M=\pm2,\pm3$. This is seen as the fine-structure lines e and f in Fig. 3. The origin of these lines can be easily understood from an inspection of Fig. 4(a), where the corresponding transitions are indicated. The EPR lines e are caused by the $M=\frac{1}{2}\leftrightarrow M'=-\frac{3}{2}$ transitions and lines f by the $M=-\frac{1}{2}\leftrightarrow M'=-\frac{5}{2}$ transitions.

The origin of the lines around the ⟨100⟩ direction, denoted g in Fig. 3, is seen in Fig. 4(b). The deviation of the experimental values from those calculated for this group is connected with its low intensity and with the problem of determining the center of gravity for the very complicated hyperfine structure.

From an analysis of the line positions as described above, it is only possible to determine the absolute value of the fine-structure parameter D. The physical relevance of the sign is illustrated in Fig. 5, where the energy-level structure for a positive value of D is shown in Fig. 5(a) and for a negative value of D in Fig. 5(b). A method to determine the sign is to calculate the intensities of EPR lines originating from different Kramers doublets and to compare the results with the experimental situation. We have chosen two lines, at $B=110$ mT corresponding to the a or a' transition in Fig. 5, and at $B=495$ mT corresponding to the b or b' in Fig. 5. The experimental data, which have been obtained between 4.5 and 40 K, are plotted as crosses (110-mT line) and open circles (495-mT line) in Fig. 5(c). The calculated, normalized EPR intensities for a negative (dashed lines) and a positive (solid lines) D value are also included in Fig. 5(c). It is clearly

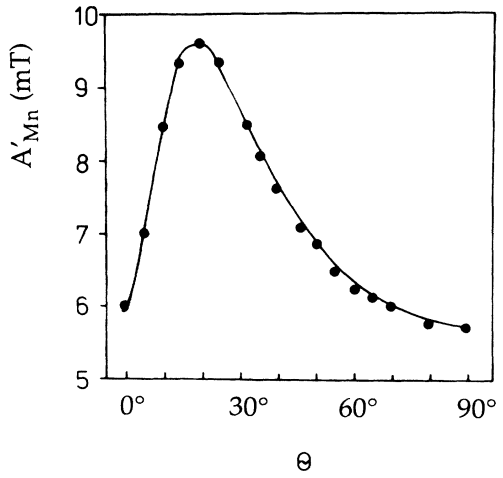

FIG. 6. Experimental (solid circles) and calculated (solid lines) angular variation of the averaged effective hyperfine splitting of the $M=\frac{1}{2}\leftrightarrow M'=-\frac{1}{2}$ transition for the $(Mn_i^{2+}In_s^{-})$ pair at 9.53 GHz and $T=4.2$ K.

seen that only the lines calculated with a positive D value satisfy the experimental data, i.e., $D=+0.52$ as given in Table I.

The averaged distances between the manganese hyperfine lines for the $|\pm 1/2\rangle$ transitions have a characteristic behavior, which is shown in Fig. 6. In the strong zero-field approximation ($D \gg g\mu_B B$), first order perturbation theory can be used to describe the observed behavior via the following equations in the $S'=\frac{1}{2}$ formalism:

$$g'^2 A'^2_{Mn} = g_{\parallel}^2 A_{Mn}^2 \cos^2\theta + k^4 g_{\perp}^2 B_{Mn}^2 \sin^2\theta \ , \quad (11)$$

$$g'^2 = g_{\parallel}^2 \cos^2\theta + k^2 g_{\perp}^2 \sin^2\theta \ . \quad (12)$$

Here, k is given by Eq. (7). The calculated dependence of the effective hyperfine splitting, using the hyperfine parameters given in Table I, is drawn as a solid line in Fig. 6. The agreement is found to be reasonable.

IV. DISCUSSION

From the experimental data on the hyperfine interactions, it was concluded that the observed EPR spectrum is caused by a pair defect consisting of one Mn and one In atom. The angular dependence of the fine structure has been argued to be determined essentially by the general feature of a manganese $3d^5$ center with a $^6S_{5/2}$ ground state in a cubic crystal field with a dominant trigonal component caused by the associated indium. The trigonal zero-field splitting energy and the Zeeman energy at the EPR transitions have, furthermore, been shown to be of the same order of magnitude, and we are therefore faced with a so-called intermediate case (see, e.g., Ref. 19). It is concluded that the microscopic structure of the defect is a pair consisting of an interstitial Mn^{2+} ion and a substitutional In^{-} ion located on the nearest-neighbor site, i.e., a $(Mn^{2+}In^{-})$ pair.

This conclusion on the microscopic structure of the defect is supported by several arguments. First, for $3d^n$ atoms, the $\frac{5}{2}$ spin system is expected only for Mn^{2+} on an interstitial site, or Mn^{2-} on a substitutional site.[1,7,8] A comparison of the spin Hamiltonian parameters, especially the hyperfine interaction parameters, for the MnIn pair on the one hand and the Mn_i^{2+} and Mn_s^{2-} on the other hand,[1] favors strongly an interstitial site for the manganese ion. Second, it is a commonly accepted fact that Mn diffuses interstitially and remains in the interstitial lattice site after the crystal is quenched from the diffusion temperature.[2] The incorporation of Mn^{2-} on a substitutional site has only been observed in n-type materials, when lattice vacancies were simultaneously created.[1,4,10] Third, indium is known to occupy a substitutional lattice site. The charge state is most probably In^{-} since the influence of indium on the electronic structure of the defect is mainly to produce a strong trigonal crystal-field distortion. This behavior is characteristic of a spin-satisfied ion. Fourth, a strong argument in favor of the $(Mn^{2+}In^{-})$ charge state is the charge compensation behavior. The EPR spectrum is observed only in strongly doped p-type samples where the indium concentration is much higher than the manganese concentration. This means that the Fermi level is pinned at the In acceptor levels, since the Mn concentration is not sufficient to compensate all In acceptors. If the In concentration is reduced close to or below the manganese concentration, the $(Mn^{2+}In^{-})$ EPR signal disappears. We conclude that the full compensation of the In acceptors leads to the occupation of the $(MnIn)^{+/0}$ levels [in our model $(MnIn)^{+}$ means the same as $(Mn^{2+}In^{-})$]. The resulting neutral charge state has, so far, never been observed by EPR. Fifth, the observed preferential formation of pairs compared to the expected statistical distribution of Mn, as well as its stability at room temperature, demonstrates the existence of a strong attractive force between manganese and indium. We suggest that the ionicity of the constituents is mainly responsible for that force.

The ionic force might also be responsible for the fact that no observations were made of the bistable properties which have been seen for many of the iron-acceptor pairs.[20,21] The physics behind bistability is that the total energy of the TM-acceptor pairs differs when the TM ion is placed in a NN or a NNN interstitial site. The configuration-coordinate diagrams for the Fe-A pairs (A = Al, Ga, and In) given in Ref. 21 show that the trigonal NN configuration is favored if one moves from the neutral $(Fe^{+}A^{-})$ to a positive $(Fe^{2+}A^{-})$ charge state. This indicates that the Coulomb force should play a more important role in the case of $(Fe^{2+}A^{-})$ pairs, keeping in mind that a pure ionic model cannot describe the physics of such transition-metal–acceptor pairs completely. It is, therefore, perhaps not surprising that the $(Mn^{2+}A^{-})$ pairs are only observed in the NN trigonal configuration, as has been reported for $(Mn^{2+}B^{-})$,[1,14] $(Mn^{2+}Al^{-})$,[1] and $(Mn^{2+}In^{-})$ (this work).

The existence of an attractive force between the indium ion and the manganese ion most probably shifts the man-

ganese slightly from its regular tetrahedral interstitial position along the C_3 axis toward the indium. Such a shift from the nearest-neighbor position, or more generally from any position allowed by the proved trigonal symmetry, cannot be excluded from the EPR measurements since the interaction with the ^{29}Si isotopes could not be resolved.

From a comparison with the literature we note that the physical behavior and microscopic models for the known Mn^{2+}-acceptor pairs are almost identical. They differ mainly in the strength of the trigonal crystal field, which is produced by the acceptors. The chemical trend seems to be as follows: the bigger the difference between the silicon atom and the replacing acceptor, the larger the trigonal distortion is and, thus, the larger the trigonal crystal field is. For instance, the zero-field splitting parameter D for $(Mn^{2+}In^{-})$ is about 10 times larger than the value determined for the $(Mn^{2+}B^{-})$ pair.[14]

Finally, it should be mentioned that the ionic model which is used to describe many of the properties of transition-metal–acceptor pairs represents an oversimplified picture and can by no means explain all the observed data. For instance, in the case of FeB (Refs. 22 and 23) and MnB (Ref. 14) it was shown that the hyperfine interactions can only be explained by also taking into account covalence effects between the constituents of the pair. The observed, strong, indium hyperfine interaction indicates that this is also the case for MnIn.

V. CONCLUSIONS

The first observation of a manganese-indium pair in silicon is reported. From an EPR investigation, the chemical identity is proved from hyperfine interactions with both manganese and indium. The defect, which is stable at room temperature, shows trigonal symmetry and an unusually complicated fine-structure behavior, which is, caused by a so-called intermediate case, i.e., the trigonal zero-field splitting energy and the Zeeman energy are of the same order of magnitude. As a result of a direct diagonalization of the energy matrix, it is shown that the experimental data can be successfully explained assuming a $^6S_{5/2}$ ground state of a Mn^{2+} ion which is split by a strongly trigonally distorted cubic crystal field caused by a nearest-neighbor In^{-} ion. Evidence for the identification of the defect as a nearest-neighbor $(Mn_i{}^{2+}In^{-})$ pair is given.

ACKNOWLEDGMENTS

The authors would like to thank the groups of Dr. A. A. Lebedev (Physico-Technical Institute, Leningrad) and Professor C. A. J. Ammerlaan (University of Amsterdam) for supplying highly-indium-doped silicon, and U. Rehse for his support in the computer calculations. This work was supported by grants from the Swedish Natural Science Research Council and the Swedish National Board for Technical Development.

[1]G. W. Ludwig and H. H. Woodbury, in *Solid State Physics,* edited by F. Seitz and D. Turnbull (Academic, New York, 1962), Vol. 13, p. 223.

[2]E. R. Weber, Appl. Phys. A **30**, 1 (1983).

[3]H. Lemke, Phys. Status Solidi A **64**, 549 (1981); **76**, 223 (1983).

[4]M. Heider, H. Sitter, R. Czaputa, H. Feichtinger, and J. Oswald, J. Appl. Phys. **62**, 3785 (1987).

[5]H. Conzelmann, Appl. Phys. A **42**, 1 (1987).

[6]T. Bever, P. Emanuelsson, M. Kleverman, and H. G. Grimmeiss, Appl. Phys. Lett. **55**, 254 (1989).

[7]A. Zunger, in *Solid State Physics,* edited by H. Ehrenreich, F. Seitz, and D. Turnbull (Academic, New York, 1986), Vol. 39, p. 275.

[8]F. Beeler, O. K. Andersen, and M. Scheffler, Phys. Rev. Lett. **55**, 1498 (1985).

[9]J. Kreissl and W. Gehlhoff, Phys. Status Solidi B **145**, 609 (1988).

[10]H. Dietrich, H. Vollmer, and R. Labusch, Solid State Commun. **58**, 811 (1986).

[11]J. J. van Kooten, G. A. Weller, and C. A. J. Ammerlaan, Phys. Rev. B **30**, 4564 (1984).

[12]W. Gehlhoff, K. Irmscher, and U. Rehse, in *Defects in Semiconductors,* Vols. 38–41 of *Materials Science Forum,* edited by G. Ferenczi (Trans Tech, Aedermannsdorf, 1989), p. 373.

[13]P. Omling, P. Emanuelsson, W. Gehlhoff, and H. G. Grimmeiss, Solid State Commun. **70**, 807 (1989).

[14]J. Kreissl and W. Gehlhoff, Phys. Status Solidi B **112**, 695 (1982).

[15]W. Gehlhoff, P. Emanuelsson, P. Omling, and H. G. Grimmeiss, Phys. Rev. B **41**, 8560 (1990).

[16]K. Irmscher and J. Kreissl, Phys. Status Solidi A **116**, 755 (1989).

[17]H. Feichtinger, J. Oswald, R. Czaputa, P. Vogel, and K. Wünstel, in *Proceedings of the Thirteenth International Conference on Defects in Semiconductors,* edited by L. C. Kimerling and J. M. Parsey, Jr. (The Metallurgical Society of AIME, New York, 1984), Vol. 14a, p. 855.

[18]Note that in Ref. 14, Eq. (1) the term $25S_z^2$ is missing due to a misprint.

[19]R. A. Serway, W. Berlinger, K. A. Müller, and R. W. Collins, Phys. Rev. B **16**, 4761 (1977).

[20]A. Chantre and D. Bois, Phys. Rev. B **31**, 7979 (1985).

[21]A. Chantre and L. C. Kimerling, in *Defects in Semiconductors,* Vols. 10–12 of *Materials Science Forum,* edited by H. J. von Bardeleben (Trans Tech, Aedermannsdorf, 1986), p. 387.

[22]W. Gehlhoff and K. H. Segsa, Phys. Status Solidi B **115**, 443 (1983).

[23]L. V. C. Assali and J. R. Leite, in Ref. 12, p. 409.